Liquid Crystals
Publication details, including instructions for authors and subscription information:
http://www.informaworld.com/smpp/title~content=t713926090

Arch-texture in cholesteric liquid crystals

J. Baudry[a]; M. Brazovskaia[ab]; L. Lejcek[ac]; P. Oswald[a]; S. Pirkl[ad]
[a] Laboratoire de Physique, Ecole Normale Supérieure de Lyon, Lyon Cedex, France [b] Laboratoire de Physique des Solides, Université Paris-Sud, Orsay Cedex, France [c] Institute of Physics, Czech Acad. Sci., Prague, Czech Republic [d] Department of Physics, University of Pardubice, FES, Pardubice, Czech Republic

To cite this Article Baudry, J. , Brazovskaia, M. , Lejcek, L. , Oswald, P. and Pirkl, S.(1996) 'Arch-texture in cholesteric liquid crystals', Liquid Crystals, 21: 6, 893 — 901
To link to this Article: DOI: 10.1080/02678299608032907
URL: http://dx.doi.org/10.1080/02678299608032907

LIQUID CRYSTALS, 1996, VOL. 21, NO. 6, 893–901

Arch-texture in cholesteric liquid crystals

by J. BAUDRY*, M. BRAZOVSKAIA†, L. LEJCEK‡,
P. OSWALD and S. PIRKL§

Laboratoire de Physique, Ecole Normale Supérieure de Lyon, Allée d'Italie, Lyon, Cedex, France

(*Received 27 June 1996; accepted 24 July 1996*)

We have observed an arch-texture in cholesteric liquid crystals sandwiched between two glass plates making a small wedge angle. The anchoring is homeotropic on one plate and planar on the opposite one. This texture is locally periodic and composed of parallel stripes whose average direction rotates by 180° each time the sample thickness increases by $p/2$, where p is the equilibrium pitch of the cholesteric phase. This texture is due to a periodic modulation of the elastic boundary layer which forms near the plate treated for homeotropic anchoring.

1. Introduction

In this article we describe an arch-texture that we have observed in a wedge shaped hybrid cell filled with a cholesteric liquid crystal.

We recall that similar textures have already been reported in the literature, but they were observed under different experimental conditions. For instance, a pattern of *arceaux* was observed at the free surface of a droplet of a cholesteric liquid crystal deposited on a glass plate treated for planar anchoring. This texture is visible at the edge of the droplet, i.e. in a region where the thickness rapidly increases. In this experiment, the molecules at the free surface are arranged in *arceaux* which can be displayed by a decoration technique consisting of labelling the director field lines with micro-precipitates or bubbles [1, 2]. A similar pattern was also found in electron micrographs of oblique sections of crab body carapace formed by alternate layers of fibrils organized with helicoidal order, like the molecules in a cholesteric liquid crystal [3, 4].

In our experiment, the liquid crystal is sandwiched between two glass plates. The anchoring is planar on the lower plate and homeotropic on the upper one (hybrid cell). The latter boundary condition is different from that imposed at a free surface, where the anchoring is planar and degenerate, the molecules freely rotating about the normal to the surface. We thus expect that the cholesteric helix is much more distorted in a hybrid cell than in a droplet with a free surface. More precisely, we propose that the planar helicoidal structure, which develops in the bulk from the lower plate, matches to the anchoring at the upper plate within an elastic boundary layer in which the director passes from a planar orientation to one that is homeotropic. We further show that this boundary layer has a 3D structure which modulates to form the semi-circular stripes of the arch-textures observed in the wedge samples. We emphasize that this modulation of the director field does not exist in a free droplet where the *arceaux* must be artificially decorated to become visible. On the other hand, we note that in both cases, the anchoring is rotationaly degenerate at the upper surface, and this is essential to observe an arch-texture.

The plan of the article is the following. In § 2, we describe the arch-texture observed in hybrid wedge cells. These observations are complemented by precise measurements, as a function of the sample thickness, of the stripe wavelength and of the angle between the stripes and the easy anchoring direction on the lower plate. These measurements were performed in a special electro-optic cell equipped with parallel electrodes whose separation could be continuously changed. In § 3, we propose a geometrical model on the unit sphere S_2 which qualitatively explains the arch-texture.

2. Experimental observations

In order to observe the arch-texture, we prepared wedge samples between two flat glass plates. The plates are 3 mm thick and are polished to $\lambda/20$. The lower plate is coated with polyvinylic acid (PVA) which is then rubbed in a single direction. This treatment gives a planar anchoring with the molecules parallel to the rubbing direction, which is itself chosen parallel to the

* Author for correspondence.

† Permanent address: Laboratoire de Physique des Solides, Bât. 510, Université Paris-Sud, 91405 Orsay, Cedex, France

‡ Permanent address: Institute of Physics, Czech Acad. Sci., Na Slovance 2, 180 40 Prague 8, Czech Republic

§ Permanent address: University of Pardubice, FES, Department of Physics, 530 09 Pardubice, Czech Republic

0267–8292/96 $12·00

edge of the dihedron. The upper plate is coated with silane ZLI 3124 (E. Merck) to obtain a strong homeotropic anchoring (molecules normal to the surface). The cholesteric liquid crystal was prepared by mixing 2·19% by weight of the chiral mesogen CB15 (E. Merck) to the liquid crystal 8CB (4-*n*-octyl-4′-cyanobiphenyl from E. Merck). The wedge is obtained by inserting a spacer between the two glass plates on one side of the sample. The spacer is a nickel wire of diameter $d=75\,\mu m$. The angle Ω of the wedge is known by measuring through the microscope the distance D between the spacer and the edge of the dihedron: $\Omega = d/D$. In the following, $D=23{\cdot}4\,mm$ and $d=75\,\mu m$, which gives $\Omega = 0{\cdot}184°$. The sample is filled by capillarity at 38°C. The texture which is obtained after filling contains many defects (disclination lines) which are very difficult or impossible to eliminate, even after a long recovery time. For this reason, we used a directional solidification apparatus [5] to control better the growth of the cholesteric phase and decrease the number of textural defects. In this experiment the sample is first placed in the cold oven at 20°C, where it is in the smectic A phase. In this phase, the layers spontaneously orient parallel to the glass plates (homeotropic sample). Then, the cholesteric phase is grown from the smectic phase by slowly pushing the sample at a velocity $V\approx 1\,\mu m\ s^{-1}$ into the hot oven at 38°C. The temperature gradient in the gap between the two ovens is $G\approx 17°C\,cm^{-1}$. The arch-texture obtained in this way is shown in figure 1. It is composed of semicircular stripes which stack in wide equidistant bands parallel to the edge of the dihedron. The wavelength Λ/p of the stripes has been measured in the middle of each band as a function of the local sample thickness D. At these places, there is no edge dislocation in the stripe pattern and the wavelength can be precisely measured. We also found that the local sample thickness in the middle of each band is close to a multiple of $p/2$, where p is the equilibium pitch of the cholesteric phase measured by using the traditional Grandjean–Cano method ($p=15\,\mu m$ at $T=38°C$). Note that, in figure 2, we do not report any measurements below $D=1{\cdot}5p$ because the optical contrast of the stripes becomes so low that it is difficult to measure their wavelength. This figure shows that Λ/p increases when the sample thickness increases and saturates at very large thickness.

To complete this work, we performed similar experiments in an electro-optic cell equipped with two parallel electrodes whose separation D can be continuously changed. As before, the anchoring is planar on the lower electrode and homeotropic on the upper one. The cholesteric mixture is the same and the temperature, controlled to 0·1°C, is set to 38°C. The two electrodes are parallel to 10^{-4} rad. Their distance D can be changed using three differential screws and is measured to 0·1 μm with

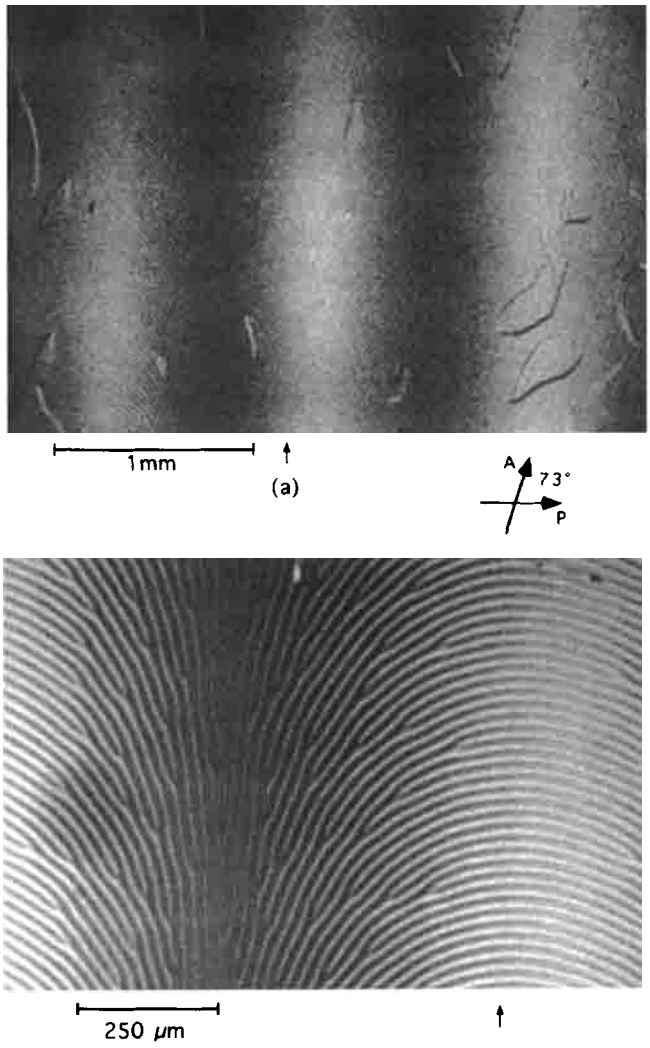

Figure 1. Photograph of the arch-texture in a wedge hybrid cell; at the arrow location the thickness is equal to 3·23*p*. (*a*) Overall view showing three bands of archs; the thickness variation from left to right equals $3p/2$. (*b*) Detail of the modulation in the arch-texture.

an LVDT (linear variable differential transformer). Observations are made between crossed polarizers. In order partly to remove the defects which occur during the cell filling, a high-frequency a.c. electric field (5 kHz) was applied. Its amplitude must be large enough to unpin the disclination lines from either dust particles or chemical inhomogeneities of the surfaces, and small enough not to unwind completely the helical structure. Another method of eliminating the lines consists of tapping on the cell to induce oscillating flow in the sample. In this way, defect-free textures can be obtained with all the stripes oriented in a well-defined direction.

In the following we call β_0 the angle between the wave

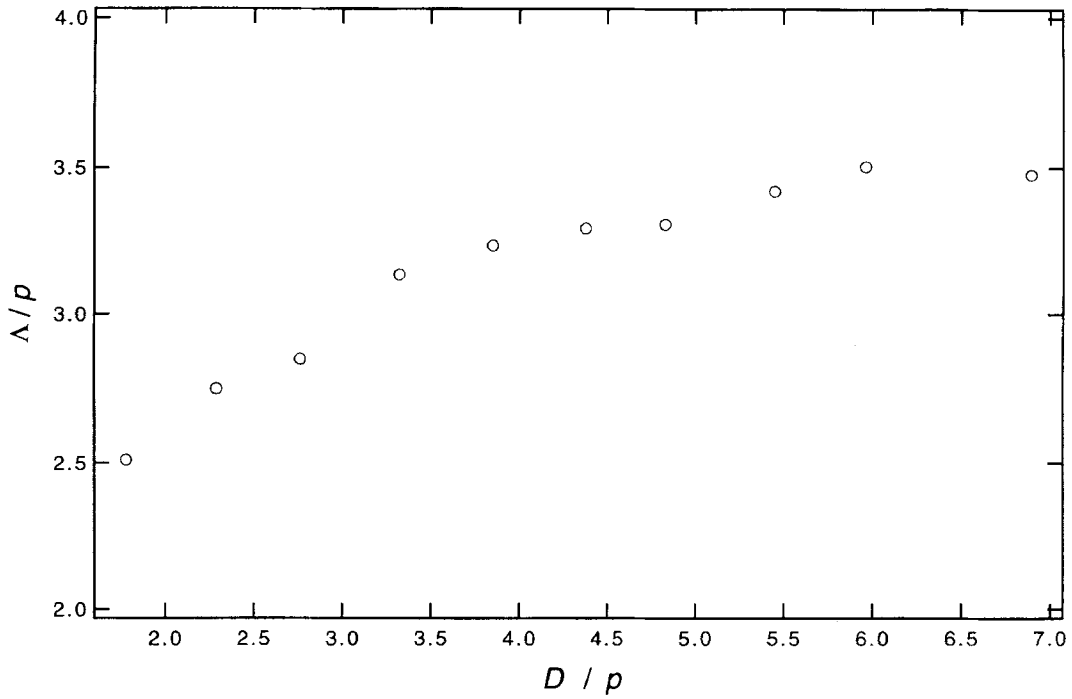

Figure 2. Stripe wavelength Λ/p measured in the middle of each band of archs as a function of the local thickness D of the sample (wedge geometry).

vector of the stripes and the direction of the planar anchoring on the lower plate, and Λ their wavelength. We measured Λ/p (figure 3(*a*)) and the angle β_0 (figure 3(*b*)) as a function of the sample thickness D.

These measurements are unambiguous as long as D/p is smaller than 5. In this range of thickness, Λ/p increases (on average) from 2·5 to 3·5, in good agreement with the previous measurements for a wedge configuration. On the other hand, the results of wavelength measurements are much more dispersed in this geometry than in the wedge. This observation suggests that the wavelength is better selected in the presence of a thickness gradient. We also observed that, in this range of thicknesses, the angle β_0 linearly varies with the thickness, which explains the appearance of an arch-texture in a wedged sample. Finally, the stripes recover the same orientation each time that the thickness increases by $p/2$. Note that the stripes are almost parallel to the anchoring direction when the thickness is a multiple of $p/2$, but this is certainly fortuitous.

The situation surprisingly becomes more complicated when the thickness is larger than $5p$. Indeed, we see in figure 4 that the texture can strongly differ from the simple stripe pattern for precise values of the thickness which are close to $n(p/2)+p/4$ (n integer). In this case, a double lattice of stripes occurs consisting of long bright lines separating narrow regions in which another system of stripes of well-defined wavelength is visible. This second system corresponds to the usual one. Its wavelength is constant and equal, within experimental error, to the value at saturation, $3{\cdot}5p$ found in the arch-texture. Also, the average orientation of these stripes is compatible with that of the stripes of the arch-texture. In figures 3(*a*) and 3(*b*), we reported the values of Λ and β_0 corresponding to these stripes. By contrast, a simple pattern of parallel stripes is observed at intermediate thicknesses close to $n(p/2)$ (n integer), of the same wavelength $\Lambda \approx 3{\cdot}5p$ and angle β_0 as in the arch-texture.

In order to know whether this double pattern corresponds to an equilibrium state of the system, we left the sample at rest for a long time (one day). We observed that the 'normal' stripes tend to grow, but we were not able to eliminate completely the bright lines. Nevertheless, we think that this double lattice of stripes is transient (perhaps metastable) and certainly due to the flow which is generated when the thickness is changed.

3. Simplified model of the stripe pattern

In this section, we consider a cholesteric liquid crystal confined between two parallel plates. The anchoring is planar on the lower plate and homeotropic on the upper one. We assume that the sample is composed of two parts: (1) a lower part which has a nearly ideal planar helicoidal structure which develops from the lower plate; (2) an upper part, called the elastic boundary layer, in which the molecules pass from a planar orientation to a homeotropic orientation on the upper plate (figure 5).

Our goal is, first, to show the existence of this

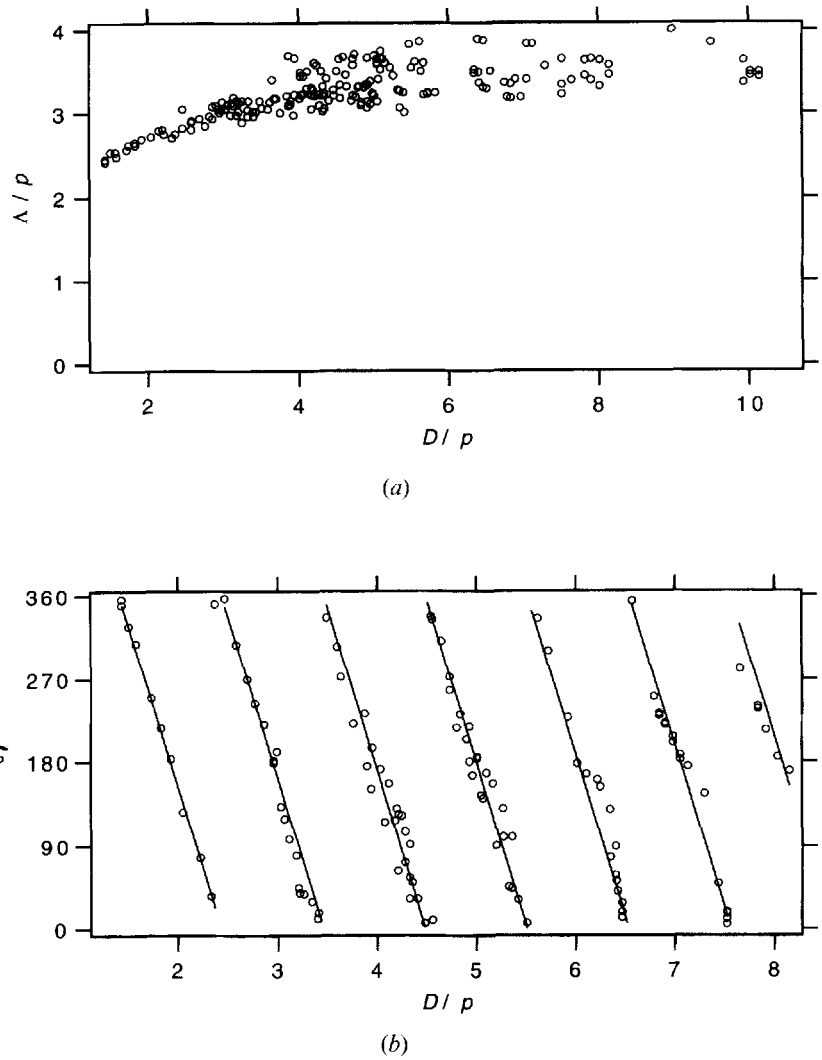

Figure 3. Stripe wavelength Λ/p (*a*) and angle β_0 (*b*) as a function of the sample thickness D (parallel geometry). Note that, although β_0 is defined *modulo* π, β_0 is plotted for more clarity between 0 and 2π in all the figures.

boundary layer and, second, to analyse its stability with respect to a 3D modulation, in order to explain the stripe texture which is observed experimentally.

3.1. *The boundary layer*

In this sub-section, we choose the z-axis perpendicular to the plates and the x-axis parallel to the molecules on the lower plate. We also assume that the director field is translationaly invariant in the horizontal plane. We call $\alpha(z)$ the tilt angle of the molecules with respect to the z-axis and $\beta(z)$ the azimuthal angle. The director field is given by:

$$\begin{aligned} n_x &= \sin\alpha(z)\cos\beta(z), \\ n_y &= \sin\alpha(z)\sin\beta(z), \\ n_z &= \cos\alpha(z), \end{aligned} \tag{1}$$

Let D be the total sample thickness and d the thickness of the elastic boundary layer. The lower plate is at $z=0$. The exact solution to this problem can be found by minimizing the Frank elastic energy. It is known and given in ref. [6]. Unfortunately, its analytical expression is too complicated to be useful in a stability analysis. For this reason, we approximate the exact solutions $\alpha(z)$ and $\beta(z)$ by the linear functions:

$$\begin{aligned} &\beta(z) = q'z \quad \text{for} \quad 0 \leqslant z \leqslant D \\ &\alpha(z) = \frac{\pi}{2} \quad \text{for} \quad 0 \leqslant z \leqslant D-d \\ &\alpha(z) = \frac{\pi}{2d}(D-z) \quad \text{for} \quad D-d \leqslant z \leqslant D \end{aligned} \tag{2}$$

where q' is the twist in the z-direction and d the thickness of the boundary layer (figure 5). They are obtained by minimizing the total elastic energy:

$$F_{\text{tot}}(d, q') = \int_0^D f \, \mathrm{d}z \tag{3}$$

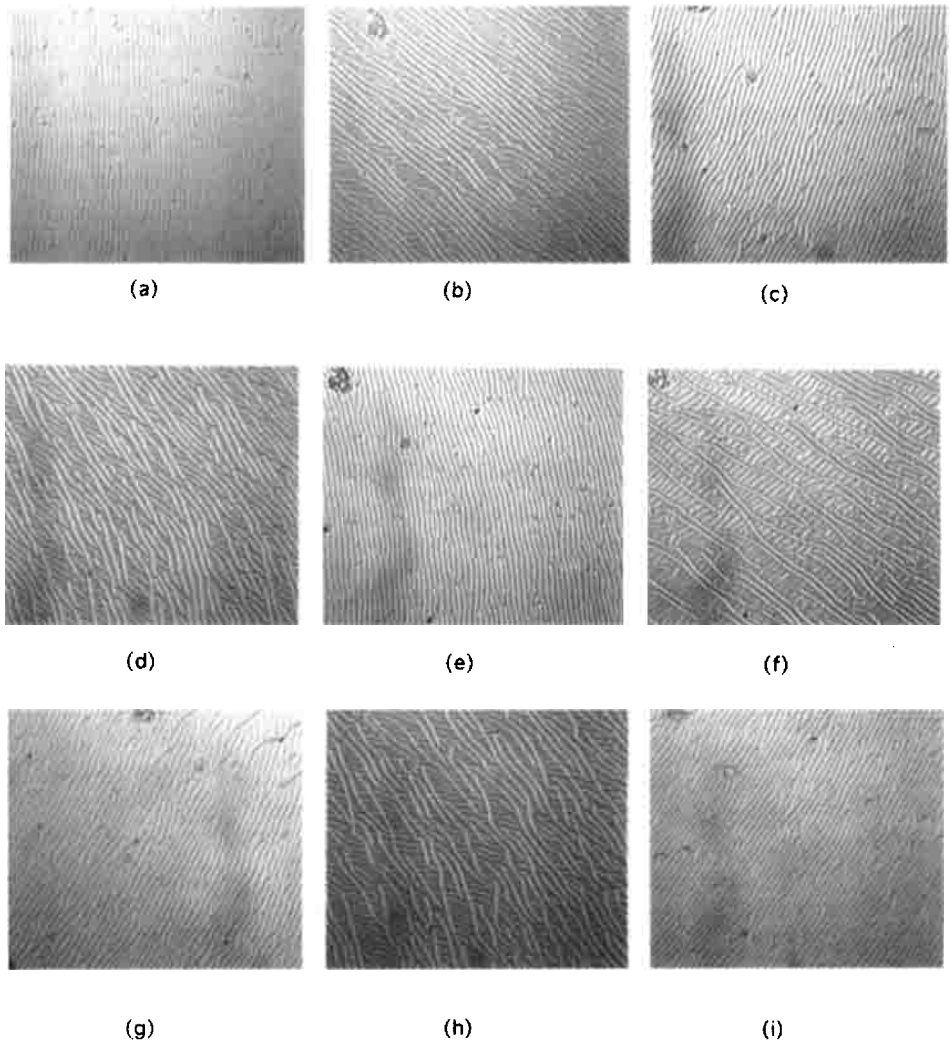

Figure 4. Textures observed in thick samples ($D/p > 5$) prepared between two parallel electrodes when (*a*) $D/p = 6{\cdot}02$; (*b*) $D/p = 6{\cdot}35$; (*c*) $D/p = 6{\cdot}47$; (*d*) $D/p = 6{\cdot}67$; (*e*) $D/p = 7{\cdot}13$; (*f*) $D/p = 7{\cdot}43$; (*g*) $D/p = 7{\cdot}52$; (*h*) $D/p = 7{\cdot}65$; (*i*) $D/p = 7{\cdot}9$. Note that a double lattice of stripes systematically appears for special values of D/p close to $n/2 + 1/4$ (n integer).

where

$$\frac{f}{K_2} = \frac{K_{12}}{2}(\text{div } \mathbf{n})^2 + \frac{1}{2}(q + \mathbf{n}.\text{curl } \mathbf{n})^2 + \frac{K_{32}}{2}(\mathbf{n} \times \text{curl } \mathbf{n})^2 \tag{4}$$

is the Frank energy. In this expression, $K_{12} = K_1/K_2$ and $K_{32} = K_3/K_2$ are the ratios of the elastic constants and $q = 2\pi/p$. A straightforward calculation gives:

$$\frac{p}{2K_2\pi^2} F_{\text{tot}}(d, q') = d\frac{p' - p}{pp'} + \frac{p}{32d}(K_{12} + K_{32}) + \frac{dp}{8p'^2}(3 + K_{32}) + (D - d)\frac{(p' - p)^2}{pp'^2} \tag{5}$$

For a thick sample ($D \gg p$), the minimization with respect to p' and d gives:

$$p' \approx p \tag{6a}$$

$$d \approx \frac{p}{2}\left(\frac{K_{12} + K_{32}}{3 + K_{32}}\right)^{1/2} \approx \frac{p}{2} \tag{6b}$$

This very simple calculation shows the existence of a boundary layer of typical thickness $p/2$ in which the molecules pass from planar to homeotropic orientation. Outside this boundary layer the cholesteric phase is distorted very little. These results are in good qualitative agreement with the exact solution.

In the following sub-section, we show that this solution is unstable with respect to some special modulations of the director field in the horizontal plane.

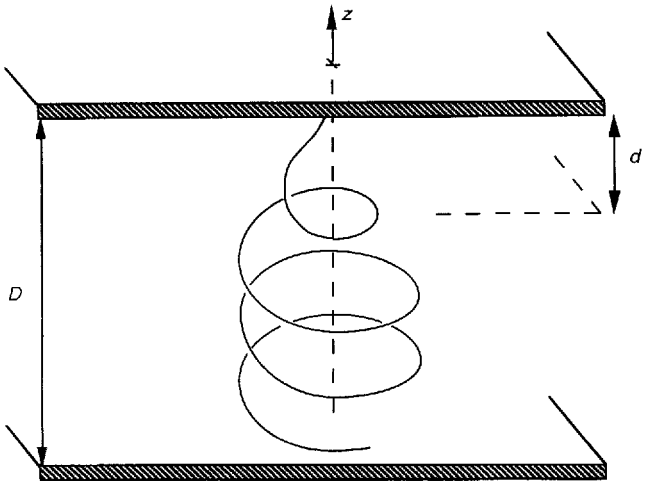

Figure 5. Schematic representation of the cholesteric helix in a hybrid sample. In the lower part of the sample (of thickness $D-d$), the director is in a planar orientation and the cholesteric helix is very little distorted. The director rotates to match the homeotropic anchoring at the upper plate within the elastic boundary layer of thickness d.

3.2. *Stability analysis*

The experiment shows that the boundary layer modulates in a well-defined direction with respect to the direction of planar anchoring on the lower plate. In the following, the x-axis is chosen parallel to the wave vector $\mathbf{k}$ of this modulation and we call β_0 the angle between the x-axis and the direction of planar anchoring on the lower plate.

In order to describe this modulation, we use the representation on the unit sphere S_2 of the director field. This method has already been used to describe the cholesteric fingers which form between two parallel plates treated in homeotropic anchoring [7–9]. Briefly, it consists of associating a trajectory in real space with a trajectory on the sphere. In our case, the director field in the boundary layer is completely known as long as we know the image of every line parallel to the x-axis. Without modulation, the image of such a line is a point with angular coordinates $\alpha(z)$ and $\beta(z)$. In the presence of a modulation, this point is replaced by a closed trajectory which we suppose to be a small circle of 'angular radius' $\gamma(z)$ (figure 6(*a*)). Because of the homeotropic anchoring on the upper plate, $\gamma(z)$ must vanish at $z=D$. We make the same assumption at $z=D-d$ (bottom limit of the boundary layer). We also assume that the director traces out this circle at 'constant velocity' $\phi=k.x$. With this choice of distortion, the director field in the real space becomes:

$$\begin{aligned} n_x &= [\cos(\alpha+\gamma)\cos\beta\cos\phi-\sin\beta\sin\phi]\sin\gamma \\ &\quad +\sin(\alpha+\gamma)\cos\beta\cos\gamma, \\ n_y &= [\cos(\alpha+\gamma)\sin\beta\cos\phi+\cos\beta\sin\phi]\sin\gamma \\ &\quad +\sin(\alpha+\gamma)\sin\beta\cos\gamma, \\ n_z &= -\sin(\alpha+\gamma)\cos\phi\sin\gamma+\cos(\alpha+\gamma)\cos\gamma. \end{aligned} \tag{7}$$

Before calculating the total energy (3), we still need to define analytical expressions for angles α, β and γ. For simplicity, we have chosen linear dependences of

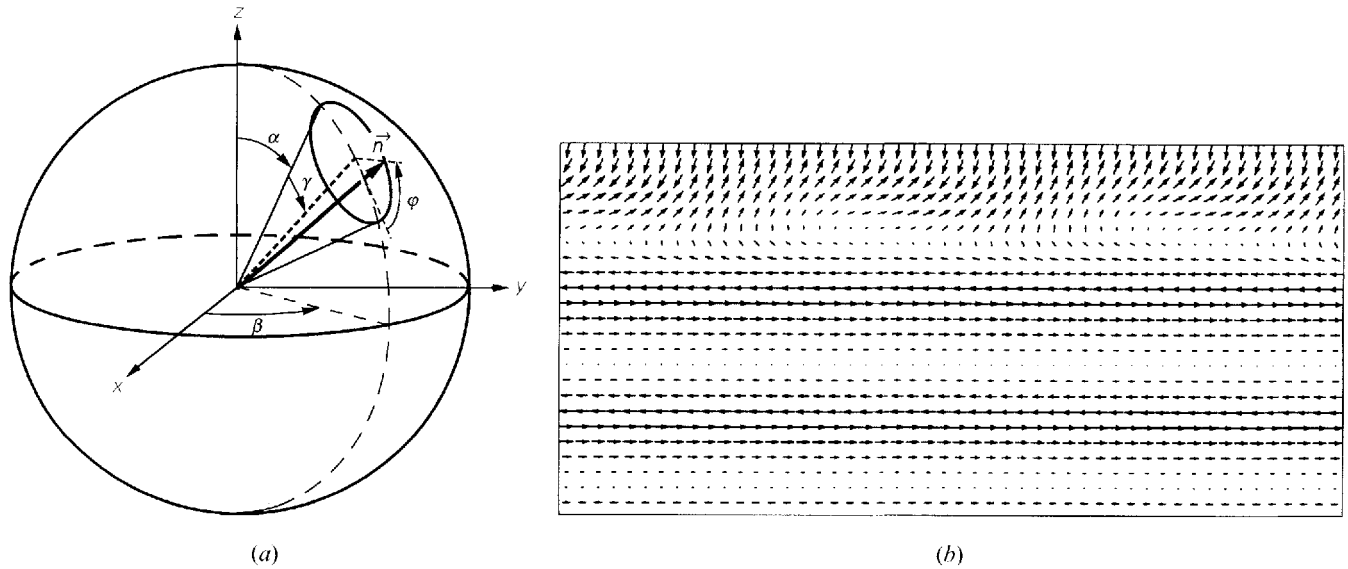

(*a*) (*b*)

Figure 6. (*a*) Definition of angles α, β, γ and ϕ in the elastic boundary layer. By moving along the x-axis, the director describes a cone of half-apex-angle γ; its axis is inclined with respect to the z-axis of angle $\alpha+\gamma$. (*b*) Director field in real space (section in a plane perpendicular to the stripes) calculated with $D/p=1{\cdot}5$, $d/p=0{\cdot}5$, $\gamma=17^\circ$ and $\beta_0=160^\circ$ (schematic).

the form:

$$\beta(z) = q'z + \beta_0 \quad \text{for} \quad z \in [0, D] \tag{8}$$

$$\gamma(z) = 0 \quad \text{for} \quad z \in [0, D-d] \tag{9a}$$

$$\gamma(z) = \frac{2\gamma_0}{d}(z - D + d) \quad \text{for} \quad z \in [D-d, D-d/2] \tag{9b}$$

$$\gamma(z) = \frac{2\gamma_0}{d}(D - z) \quad \text{for} \quad z \in [D-d/2, D] \tag{9c}$$

Angle $\alpha(z)$ is given by equation (2). In these formulae, γ_0 is the half-apex-angle of the cone described by the director in the middle plane of the boundary layer, q' the twist along the z-axis and β_0 the angle between the wave vector $\mathbf{k}$ of the modulation and the direction of planar anchoring on the lower plate. The corresponding director field is represented in figure 6(*b*).

A careful examination of the total energy per unit surface area:

$$F_{tot}(\beta_0, \gamma_0, k, d, q') = \frac{1}{\Lambda}\int_{D-d}^{D} dz \int_0^{\Lambda} dx\, \rho f + \frac{1}{2} K_2 \int_0^{D-d} dz (q - q')^2 \tag{10}$$

shows that it can be written in the form:

$$F_{tot}(\beta_0, \gamma_0, k, d, q') = \alpha(\beta_0, \gamma_0, d, q') + b(\beta_0, \gamma_0, d, q')k + c(\beta_0, \gamma_0, d, q')k^2 + \frac{1}{2} K_2 (D-d)(q - q')^2 \tag{11}$$

Its minimization with respect to k gives:

$$k = -b(\beta_0, \gamma_0, d, q')/2c(\beta_0, \gamma_0, d, q') \tag{12a}$$

and, after substitution into equation (11):

$$F_{tot}(\beta_0, \gamma_0, d, q') = a(\beta_0, \gamma_0, d, q') - b^2(\beta_0, \gamma_0, d, q')/4c(\beta_0, \gamma_0, d, q') + \frac{1}{2} K_2 (D-d)(q + q')^2 \tag{12b}$$

The last stage consists of calculating functions a, b and c and then of minimizing F_{tot} as a function of the four parameters β_0, γ_0, d and q' (with the constraint $d \leqslant D$). This can be easily done using *Mathematica* [10]. We did our calculations with $K_{12} = K_1/K_2 \approx 2$ and $K_{32} = K_3/K_2 \approx 2$, the values we found for 8CB at 38°C [11]. The main result is that the numerics converge whatever the thickness toward a minimum of energy which corresponds to a modulated structure. This is in good agreement with the experiments. On the other hand, the constraint $d \leqslant D$ forces us to consider two ranges of thicknesses.

At 'large' thickness ($D \geqslant 0{\cdot}54p$), the minimization can be performed by leaving free all the parameters. In this case, the sample is composed of two parts: the boundary layer which is modulated and the cholesteric phase which is below and very little distorted. In this regime, the wavelength Λ of the modulation is almost constant and close to $2p$ (it increases from $1{\cdot}88p$ to $1{\cdot}92p$, figure 7(*a*)). Similarly, angle γ_0 is almost constant and close to 0·2 rad (figure 7(*b*)). Finally, angle β_0 linearly varies with the sample thickness D, changing by π each time that the thickness increases by $p/2$ (figure 7(*c*)).

At small thickness ($D < 0{\cdot}54p$), a straightforward minimization of the total energy (12(*b*)) leads to $d > D$, which does not make sense. Consequently, we put $D = d$ and we minimize with respect to other variables. In this case, we found that there still exists a modulation of vanishing amplitude γ_0, but finite wavelength Λ, when D tends to zero (figure 7(*d–f*)).

In conclusion, this model qualitatively explains the formation of the stripes and their bending into semicircles in the arch-textures of the wedge samples. It confirms that the arch periodicity corresponds to a sample thickness variation of $p/2$. Consequently, this method can be used instead of the Grandjean–Cano method for measuring the equilibrium pitch of a cholesteric phase. The model also predicts that the stripe wavelength decreases at small thickness and tends to a constant value at large thickness, which is qualitatively correct. On the other hand, the calculated wavelength is too small by a factor 2. This is due to the rough approximations of the model which accounts poorly for the interactions between the boundary layer and the underlying cholesteric phase. In particular, this model seems clearly to under-estimate the thickness of the elastic boundary layer. Indeed, holding $d \approx 1{\cdot}5p$ in the model leads to a wavelength which is in good agreement with the experimental data.

4. Concluding remark

When the sample is not carefully prepared, many disclination lines delineating striped domains with different orientations are visible. If the wavelength of the stripes is the same in the different domains (within experimental error), their mean orientations are not. Typically, the misfit angle $|\Delta\beta_0|$ between the mean orientations of the stripes in two adjacent domains is about 20° in a sample of thickness $D \approx 2{\cdot}4p$ (figure 8).

In order to calculate the order of magnitude of $\Delta\beta_0$, we suppose that the line defect is an edge dislocation of

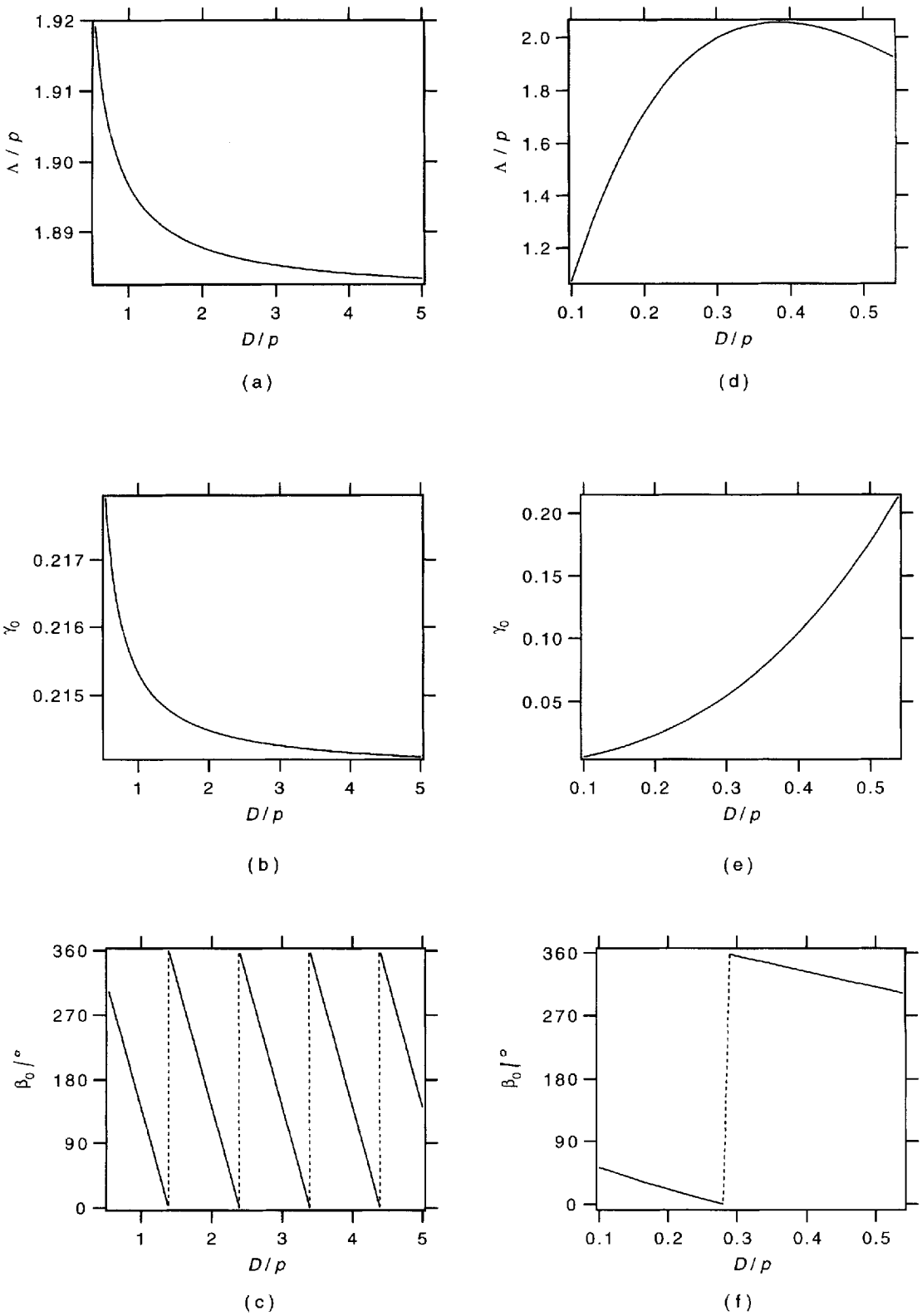

Figure 7. Wavelength Λ, angle γ_0 (giving the amplitude of the modulation) and angle β_0 (giving the direction of modulation) as a function of D/p. (*a–c*) $D/p > 0{\cdot}54$; (*d–f*) $D/p < 0{\cdot}54$.

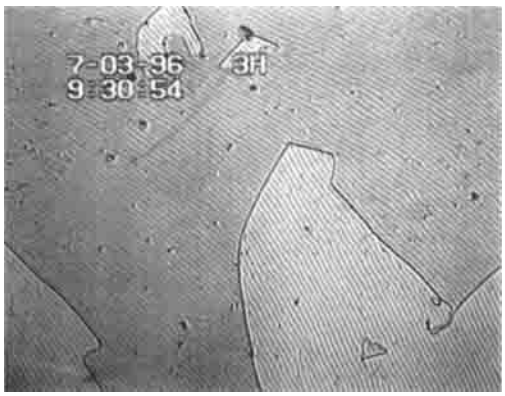

(a)

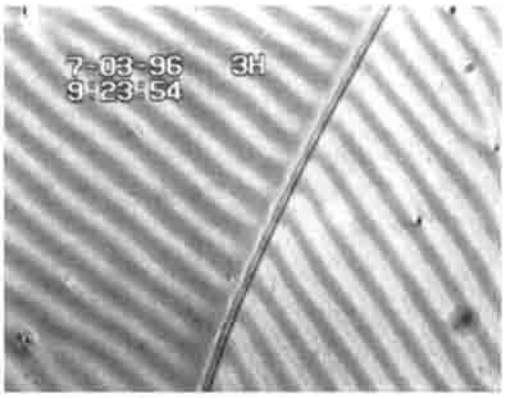

(b)

Figure 8. Disorientation of the stripes on both sides of a $p/2$-dislocation (χ-line). (*a*) Global view of a sample of thickness $D/p=2{\cdot}35$; many dislocations lines are present, they are pinned to the dust particles which are numerous in this sample. (*b*) Detail of the boundary between two domains; the misfit angle $\Delta\beta_0$ of the stripes is close to 20°.

Burgers vector $b=\pm p/2$ (χ-lines [12]). This line separates two domains: one, supposed to be at equilibrium, in which we calculate $p'/p=1{\cdot}03$ with $\Lambda=1{\cdot}88p$ and $\beta_0=-0{\cdot}42$ rad, and another, in which the number of layers is, for example, increased by one unit. In this domain, we have $p'/p\approx 2{\cdot}4/2{\cdot}9=0{\cdot}83$, and we calculate, by minimizing the total energy with p'/p constant, $\Lambda=1{\cdot}84p$ and $\beta_0=-0{\cdot}09$ rad. This calculation shows that the wavelength does not change significantly and that the stripes rotate by an angle $\Delta\beta_0=-0{\cdot}33\,\text{rad}=-19°$ across the line. The same calculation, with a layer missing, leads to a rotation of the stripes by an angle $\Delta\beta_0=18°$ and to a stripe wavelength $\Lambda=1{\cdot}93p$. These predictions are in good qualitative agreement with the experimental observations.

This work has been supported by DRET contract No 95-1117. One of us (L. L.) thanks the Ministère de l'Education Nationale for his P.A.S.T. position. It is a pleasure to thank P. C. W. Holdworth for a critical reading of the manuscript.

References

[1] CLADIS, P., KLÉMAN, M., and PIERANSKI, P., 1976, *C.R. Acad. Sci. Paris*, **273**, 275.
[2] DE GENNES, P. G., and PROST, J., 1993, *The Physics of Liquid Crystals*, 2nd Edn., (Oxford: Clarendon Press).
[3] BOULIGAND, Y., 1969, *J. Physique Colloque. C4*, **30** (Supp. no. 11–12), C4.
[4] BOULIGAND, Y., 1978, *Liquid Crystals*, Solid State Physics, Vol. 14, edited by L. Liebert, (New York: Academic Press), p. 259.
[5] OSWALD, P., MOULIN, M., METZ, P., GÉMINARD, J. C., SOTTA, P., and SALLEN, L., 1993, *J. Phys. III Fr.*, **3**, 1891.
[6] FISCHER, F., 1976, *Z. Naturfirsch.*, **31a**, 41.
[7] LEQUEUX, F., OSWALD, P., and BECHHOEFER, J., 1989, *Phys. Rev. A*, **40**, 3974.
[8] LEQUEUX, F., 1988, PhD thesis, Universite de Paris Sud, France.
[9] RIBIERE, P., 1992, PhD thesis, No. 289.92, Universite Claude Bernard-Lyon, France.
[10] WOLFRAM, S., 1991, *Mathematica* (Addison-Weseley).
[11] MADHUSUDANA, N. V., and PRATIBHA, R., 1982, *Mol. Cryst. liq. Cryst.*, **89**, 249.
[12] KLÉMAN, M., 1977, *Points Lignes Parois*, Vol. 1 (Orsay: Les Editions de Physique).